Polarization-dependent angular photoelectron distribution of solid C_{60}

J. Schiessling* and L. Kjeldgaard†
Department of Physics, Uppsala University, Box 530, SE-751 21 Uppsala, Sweden

T. Balasubramanian
Max-Lab, University of Lund, Box 118, SE-221 00 Lund, Sweden

J. Nordgren
Department of Physics, Uppsala University, Box 530, SE-751 21 Uppsala, Sweden

P. A. Brühwiler‡
Department of Physics, Uppsala University, Box 530, SE-751 21 Uppsala, Sweden
and EMPA, Lerchenfeldstrasse 5, CH-9014 St. Gallen, Switzerland
(Received 5 June 2003; published 5 November 2003)

We present angle- and polarization-dependent photoelectron spectra of solid C_{60} recorded over a large range of emission angles. The bands derived from the three highest molecular orbitals are very similar in their angular distribution and show a strong dependence on both light polarization direction and sample orientation. We show that a molecular emission pattern modified by solid-state effects accounts for the observations.

DOI: 10.1103/PhysRevB.68.205405 PACS number(s): 79.60.−i, 33.60.−q, 36.40.Mr

I. INTRODUCTION

Angle-resolved photoemission (ARPES) has served as the primary tool to investigate the electronic structure of novel materials for several decades.[1] Of particular current interest are correlated systems like the high-temperature superconducting oxides and molecular solids. It is the question of intensity with which photoemission experiments have the most difficulty in establishing absolute values. However, the spectral intensity constitutes one of the more interesting outputs in the study of, e.g., strongly correlated materials.[2] Recently a reexamination of the role of the light polarization clarified fundamental differences between theory and experiment for high-temperature superconductors.[3]

It is therefore clear that a detailed knowledge of the role of light polarization in solid-state photoemission is fundamental for a systematic improvement of our understanding of novel materials. Our present focus is the electronic structure of solid C_{60}, which is one of the most well-studied molecular materials. It has been a topic of immense interest in its own right,[4–6] as well as being the starting point for understanding the fulleride superconductors.[5,7,8] The difficulty in detecting solid-state effects in the line shapes of such spectra[9–13] could be taken as tacit confirmation of the proposal that, due to orientational disorder and the large unit cell, such effects should be small.[14,15]

At the same time, the molecular nature of the photon energy-[9,16] and final-state-dependent[11,13] cross sections for solid C_{60} photoelectron spectra (PES) was appreciated early on. When the same photon-energy dependencies were measured for the gas phase,[17] it became clear that the observed variations were almost unaltered between free and solid C_{60}. Another important expression of this symmetry emerges in the angular PES cross sections of gas phase C_{60}.[17–19] These results suggest that the molecular symmetry is of great importance for the electronic states up to kinetic energies of at least 100 eV,[20–22] and one can ask if this property is also preserved in the condensed phase.

We report ARPES of solid C_{60}, and detect molecular photoemission angle- and light polarization-dependent cross section variations. We find that the solid-state cross section can, to first order, be described by a molecular β parameter, which is the primary result of this work. At the same time, it is apparent that scattering in the solid significantly modifies the angular distribution. We analyze the role of inelastic scattering in a continuum model and taking the finite size of the molecules into account. We tentatively suggest that the molecular dimension could cause elastic scattering to be effectively nonisotropic for molecular solids. Finally, we point out the role of light polarization for metallic molecular systems in determining the proportion of inelastically scattered photoelectrons in PES.

II. EXPERIMENT

The experiments were carried out at Beamline 33 at MaxLab.[23] The end station is equipped with a goniometer-mounted electron energy analyzer. The emission could be varied over 2π radians, with tighter constraints for certain sample orientations. By scanning the polar angle with 6° step-size spectra were taken in the plane defined by the light polarization and incidence directions. The plane of incidence and emission was always perpendicular to the sample surface. The analyzer acceptance angle was set to $\pm 2°$. The spot size of the synchrotron light on the sample was approx $2(\mathrm{h})\times 1(\mathrm{v})$ mm^2 in normal incidence. The effective aperture of the analyzer has a diameter of 1.5 mm at the sample surface. The photon energy was 110.07 eV, calibrated by measuring the highest occupied molecular orbital (HOMO) structure excited by first- and second-order light. The kinetic-energy scale was calibrated with the ionization potential[24] of the HOMO of 6.9 eV. The overall energy resolution is 80 meV. The spectra are normalized to the light flux, which was measured as photocurrent on a gold mesh placed

in the beamline in front of the analysis chamber. The sample was prepared in a standard UHV preparation chamber with a base pressure of 4×10^{-10} mbar, the pressure of the analysis chamber was 6×10^{-11} mbar. C_{60} was sublimed from a Knudsen cell onto an atomically clean Al(110) surface, held at room temperature during deposition. The diameter of the substrate was 10 mm. Subsequent to deposition the multilayer C_{60} film was annealed for 4 min at 200 ° C. During measurements the sample was at room temperature.

III. RESULTS

Angle-dependent spectra of the bands derived from the occupied molecular orbitals (MO's) of C_{60} were taken at light polarization angles of 5° and 45° from surface normal. The spectra were normalized to the intensity of the synchrotron light and acquisition time. One set of ARPES data taken with light polarization angle of 45° is shown in Fig. 1. The overall impression from the data is that the maximum intensity is found close to the angle of light polarization. In order to quantify the angular distribution (AD), the individual spectra are modeled with Gaussians, as illustrated in Fig. 1(b). The intensity distributions of the PES peaks from the HOMO, HOMO-1, and Peak *C* for the respective light polarizations are plotted in Fig. 2. The three highest spectral features have nearly identical angular distributions. Typically, molecular AD's are displayed as polar plots. Since it is difficult to analyze line shapes in a polar plot, we display the AD in a cartesian plot and a polar plot in Fig. 2. Clearly, the ADs are largely determined by the light polarization angle. However, the AD in Fig. 2(a) is approximately symmetric with respect to the light polarization, whereas that in Fig. 2(b) is not.

For the free molecule, the AD of an emitted particle after dipole absorption is described by[25,26]

$$\frac{d\sigma}{d\Omega}=\frac{\sigma}{4\pi}[1+\beta P_2(\cos\theta)], \tag{1}$$

where σ is the total photoelectric cross section, θ denotes the angle between light polarization and photoelectron emission, and P_2 represents the Legendre polynomial of second order. β reflects the MO symmetry, and can be in the range of $-1\leqslant\beta\leqslant2$. For a kinetic energy of 103 eV, the anisotropy value for the HOMO of C_{60} is calculated[27] to be $\beta=1.1$. We expect this value to be accurate, based on the good agreement achieved in the same calculation at lower energies with experimental data.[17–19]

In a homogeneous and isotropic medium (continuum approximation), the number of photoelectrons will be attenuated proportionally to the path taken by the photoelectron on its way to the sample surface, and the number of photoelectrons dN emerging from depth z in direction α can be written as[28]

$$dN_\alpha(z)=C\left(\frac{d\sigma}{d\Omega}\right)A(\alpha)e^{-z/(\lambda\cos\alpha)}dz. \tag{2}$$

Here, α is the angle between sample normal and the direction of analysis, the constant C comprises the instrumental factors, density of the sample, and the x-ray flux. The differential cross section $(d\sigma/d\Omega)$ describes the initial molecular photoemission AD. According to geometric considerations the surface area $A(\alpha)$ intersecting the acceptance cone of the analyzer increases with the emission angle as $1/\cos\alpha$. λ is the inelastic mean-free path (imfp) which is the characteristic distance in the solid that photoelectrons travel between inelastic collisions.[29] This expression includes the assumption that inelastic scattering removes the photoelectron from the spectral region of interest and that elastic scattering can be neglected. For a semi-infinite sample the integral over all depth z gives $\int_0^\infty dz e^{-z/\lambda\cos\alpha}=\lambda\cos\alpha$. Hence, the AD from a continuous solid-state sample is proportional to the initial photoemission intensity

$$I=\int_0^\infty dN_\alpha(z)=C\left(\frac{d\sigma}{d\Omega}\right)\lambda. \tag{3}$$

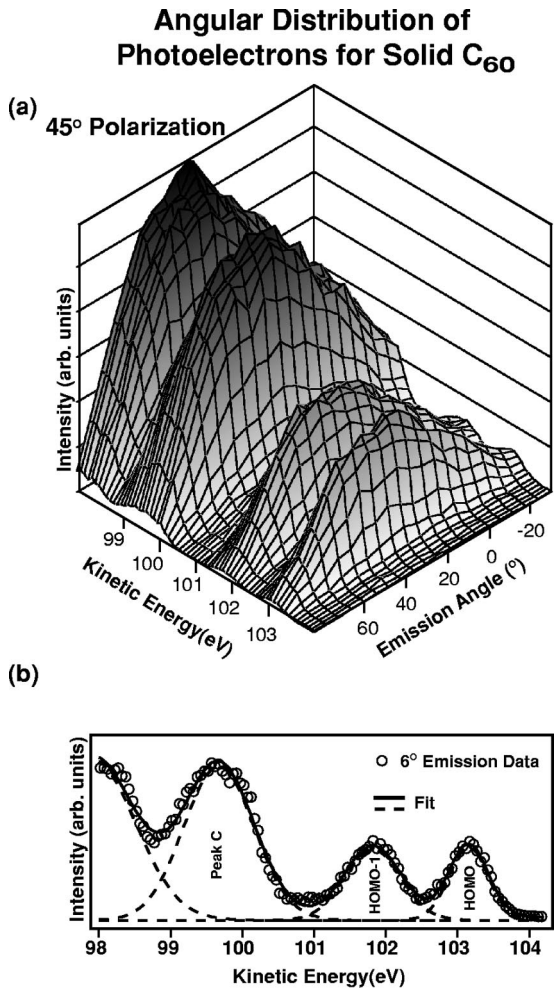

FIG. 1. (a) Angle-dependent valence PES from the three highest MO's taken with the light polarized at $+45°$. Spectra were taken at 6° intervals, and each is shown directly as a grid line along kinetic energy. The photoemission intensity is normalized to the photon flux and corrected for acquisition time. (b) The 6° emission spectrum with a fit using a series of Gaussians as shown, illustrating the method used to extract the intensity information for each peak displayed in later figures. The peak notations are in accordance with Ref. 40.

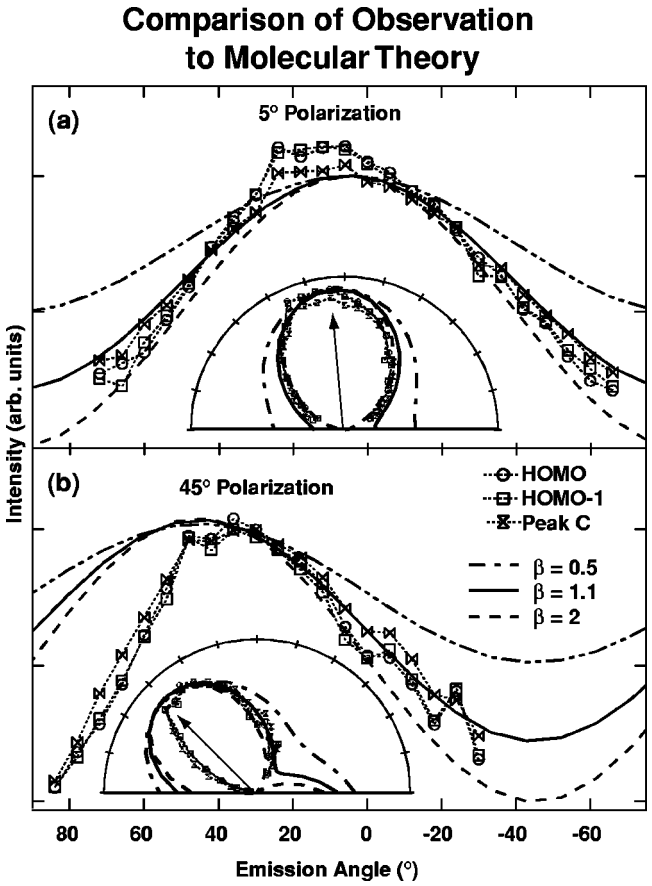

FIG. 2. Intensity derived from the spectra excited by light polarized at the indicated angle. The intensity of the HOMO, HOMO-1, and Peak *C* lines are derived from fits as illustrated in Fig. 1(b), with scaling factors applied to enable an assessment of differences among them, which are seen to be small. The experimental results are compared to distributions corresponding to the indicated molecular β values. The insets reproduce the ADs as polar plots.

In Fig. 2 we compare the present results with the molecular AD for different anisotropy values β. Overall the data are in accordance with the calculations. However, the AD's found are somewhat narrower than the calculated $\beta=1.1$. Furthermore, for 45° light polarization at positive emission angles there is an apparent cutoff in the AD. Below we try to explain these differences in terms of the following: (1) the cutoff as a geometrical limitation and (2) possible scattering effects due the finite size of the molecules.

(1) We find that the function $A(\alpha)$ plays an important role for the 45° data. It is clear that the horizontal light spot dimension of 2 mm given in Sec. II will be spread out over the sample surface by a factor of $1/\sin(\phi)$, where ϕ is the polarization angle. Likewise, the analyzer will accept electrons from the sample surface according to $1/\cos(\alpha)$. Certain limits on both of these factors occur for particular geometries. For example, when the light spot has a finite size, the acceptance function of the analyzer has an upper limit. The sample size also places upper limits on both of these factors. The results can be described in the present case as the cutoff angles α_c given in Table I, above which $A(\alpha)$ is assumed to be constant, as summarized in the following conditions

TABLE I. Illuminated sample dimension and detection cutoff angle.

ϕ	2 mm/sin ϕ	α_c
45°	2.8 mm	57.6°
5°	>10 mm	81.4°

$$A(\alpha)=\begin{cases} A_0/\cos\alpha & \alpha\leqslant\alpha_c \\ A_0/\cos\alpha_c & \alpha>\alpha_c \end{cases},$$

where A_0 is the illuminated sample area measured by the analyzer in normal emission. It is clear that for $\phi=45°$ this cutoff suggests an explanation of the major deviation between the β distributions of Fig. 2(b) and experiment. We have also considered the effects of refraction of the photoelectrons[30] on the AD. We find that refraction does not qualitatively alter the AD in the angular range of the measured distributions shown here, although there are minor quantitative changes for the largest positive angles for 45° polarization. This effect will therefore be neglected in what follows.

(2) Since the effects of α_C on $A(\alpha)$ cannot explain the narrowed AD for 5° polarization, we are led to consider other aspects of solid-state scattering. Above we have considered the solid as a continuum of emitters and scatterers. Since C_{60} is a large molecule we will investigate the effects of its size on the attenuation of the photoelectrons. Thus, we develop a very simple model of the effects of inelastic scattering on the AD including the ''granularity'' of the sample, starting with a single layer. In principle, valence electrons can be emitted from every point of the shell of the molecules with an initial AD determined by the molecular photoemission described by Eq. (1). We approximate the molecules with spheres of the C_{60} van der Waals radius[31] $R=5$ Å and place the molecules at the nearest-neighbor distance[31] of $b=10$ Å. The trajectories of photoelectrons from the point of emission towards the photoelectron analyzer are partly blocked by neighboring molecules, as shown in Fig. 3(a). The number of electrons reaching the analyzer therefore depends on the degree of blocking, here modeled as an overlap of the projection of the neighboring molecule onto the source molecule. The length $l(\alpha,m)$ which characterizes the degree of blocking can be obtained from the geometry shown in Fig. 3(a)

$$l(\alpha,m)=\begin{cases} 0 & |\alpha|\leqslant\arccos\dfrac{2R}{mb} \\ 2R-mb\cos\alpha & |\alpha|>\arccos\dfrac{2R}{mb} \end{cases}; \quad (4)$$

with $m=1,2,\ldots$ the neighbor index.

Figure 3(b) is the view perpendicular to the plane shown in Fig. 3(a). The fraction F of the source molecule which is blocked is seen to be

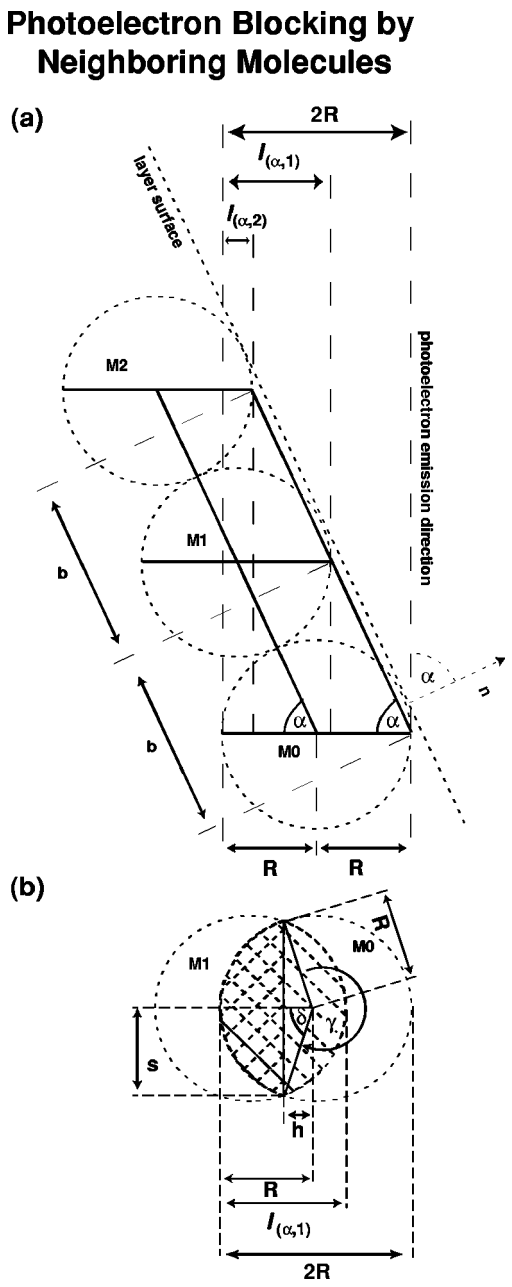

FIG. 3. Schematic of a C_{60} layer and the influence of the finite size on the photoemission intensity. The molecules are displayed as dashed circles, with a radius $R=5$ Å and neighbor distance of $b=10$ Å. (a) Side view in the figure. Molecule M0 is the emitter. For emission angles $\alpha>0$ the nearest-neighbor molecule M1 blocks M0 to a degree characterized by the length $l(\alpha,1)$. At an emission angle $|\alpha|=\arccos(2R/2b)$ the next-nearest-neighbor M2 starts to block trajectories from M0. See the text for further discussion. (b) Overlapping of molecules as seen by the photoelectron analyzer. The fractional area $F(\alpha,1)$ which is taken to be blocked in Eq. (5) is shaded. See the text for more details.

$$F(\alpha,m)=\frac{2}{\pi R^2}\left(\pi R^2-R^2\frac{\gamma}{2}+hs\right) \tag{5}$$

with

$$h=R-\frac{l}{2},$$

$$s=\sqrt{R^2-h^2},$$

$$\gamma=2\pi-2\delta=2\pi-2\arccos\frac{h}{R},$$

$$l=l(\alpha,m),\ \text{defined in Eq. (4).}$$

Still considering a given source molecule, we define the transmission function of the given layer as

$$T_{\text{intra}}(\alpha)=1-\sum_{m=1}^{\infty}[p^{m-1}F(\alpha,m)-p^mF(\alpha,m)], \tag{6}$$

where we have introduced an average blocking probability p for an electron traversing a molecule.

Equation (6) merely reflects the following summation: the transmission of the unblocked molecule M0 is 1, and the influence of a neighbor is described by the two parts of the sum. The first part subtracts the fractional overlap of M1 with M0 from the initial intensity. In the second part the reduced intensity of the blocked area is added by multiplying the fractional overlap with p.[1] The subsequent terms in the sum are obtained similarly. When $l(m,\alpha)=0$ as defined in Eq. (4), the series ends. This derivation is valid for a particular geometry, i.e., for emission along rows of molecules. For other azimuthal orientations less blocking, and a more complicated expression would be obtained.

To estimate the transmission probability p we assume an average path length of the photoelectron through an adjacent molecule of $\zeta=7$ Å and obtain a transmission probability $p=\exp(-7\ \text{Å}/\lambda)$. Overlayer core-level spectra[32] of C_{60} show that photoelectrons with a kinetic energy of 115 eV have a contribution from the first layer of 38%. Assuming an exponential decay an escape depth can be calculated. We assume that the core-level photoelectrons are emitted on average from the center of the molecules.[33] This gives an emission length of 5 Å for the first layer photoelectrons and 5 Å+8Å=13 Å for the second layer, with a layer separation[31] of 8 Å. Thus,

$$I_{1\text{st}}/I_{\text{surf}}=0.38/0.62=e^{-13\ \text{Å}/\lambda}/e^{-5\ \text{Å}/\lambda}=e^{-8\ \text{Å}/\lambda},$$

and it follows that $\lambda=16.32$ Å.

In the literature values between[36] 4 Å (escape depth) and[37] 8 Å (electron mean-free path) are reported for 100 eV kinetic-energy electrons. We will therefore employ a selection of values when testing the ''granularity'' model in what follows. It is clear without a calculation that the higher angles in a monolayer AD will be suppressed by this mechanism, as they would in the continuum model of a finite-thickness slab. Recall that the AD of the semi-infinite continuum model is independent of the imfp.

To obtain the solid-state AD the photoemission intensity from all layers in the sample has to be added, giving

$$I(\alpha)=C\left(\frac{d\sigma}{d\Omega}\right)T_{\text{intra}}(\alpha)A(\alpha)\sum_{n=0}^{\infty}e^{-(n)d/(\lambda\cos\alpha)}, \tag{7}$$

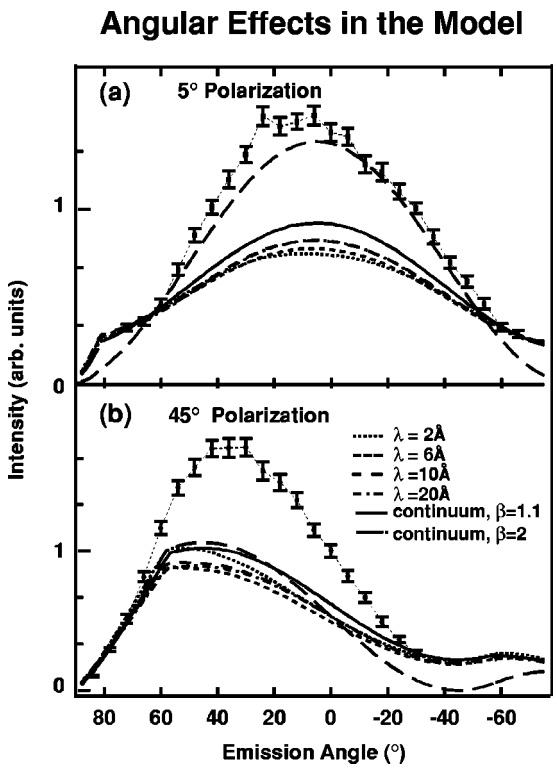

FIG. 4. Comparison of Eq. (7) for a set of imfp with the continuum approximation Eq. (3) and the experimental AD of the HOMO: (a) polarization direction 5°, (b) polarization 45°. The bars display the statistical error of the experimental data. The calculated AD's are normalized to match the experimental data at the high emission angles and are corrected for the analyzer spot cutoff. The continuum AD is shown for the predicted asymmetry parameter $\beta=1.1$, and the maximal value of $\beta=2$. The intralayer transmission probability in Eq. 6 is connected to the imfp via $p=e^{-7\text{Å}/\lambda}$. The calculated AD is only mildly sensitive to the imfp.

where $d=8$ Å is the layer spacing.[31] The resultant photoemission intensity distribution is displayed in Fig. 4 for a range of λ values. Since the model above describes the inelastic losses, it reflects the maximum intensity; thus the calculated AD's are scaled in the figure to be constrained by the experimental values. It turns out that the choice of λ has little influence on the modification of the AD in the finite-size model, just as in the continuum model.[38] Even the extreme value $\beta=2$ is not sufficient to explain the AD; see Fig. 4(b). This suggests that inelastic scattering alone is not sufficient to explain the observations. About 28% of the area below the experimental AD is not covered by the discussed models.

Elastic scattering has been shown to be important in a continuum model, easily accounting for redistributions of the AD (Ref. 39) of the order of 20%, and is an effect which tends to smear it out. However, this would not explain the deviation observed here, which tends to emphasize the high-intensity region of the expected molecular AD. Hence, we postulate that a continuum model of elastic photoelectron scattering is not adequate to account for our observations. Our primary assumption is that the value of β already includes all intramolecular effects on the AD, and we have shown that inelastic scattering does not appear to explain the observed deviations from the expected value of β, or even from the extreme value $\beta=2$ in the case of 45° polarization. It therefore seems likely that finite-size effects on the elastic scattering could play an important role. In particular, a kind of intralayer channeling effect due to the fact that a given source molecule is surrounded by a hexagon of nearest neighbors seems plausible.

Since the normal direction corresponds to the direction of least scattering, we speculate that electrons scattered into trajectories close to this direction will be favored to avoid being removed from the spectrum by inelastic scattering. A computational study of this possibility would be helpful in deciding this matter more conclusively, but is beyond the scope of the present work. We note in closing that for the 5° polarization data, the intensity is enhanced relative to the molecular AD close to the expected peak emission direction, whereas for the 45° polarization data, the enhancement is between normal and the polarization direction, which would seem to allow the mechanism tentatively proposed here.

IV. CONCLUSIONS

We observe a photoelectron intensity AD of solid C_{60} for $h\nu=110$ eV qualitatively quite close to the expectations for free molecules. In addition to inelastic-scattering effects, angular cutoff effects due to the sample illumination and photoelectron collection geometries are shown to be important. The difference between the observed and molecularly modeled AD's suggests that solid-state effects are significant. However, the observation is not in accordance with expectations of a continuum model of isotropic incoherent scattering. We tentatively suggest that elastic scattering in the sample brings about a channeling of the photoelectrons towards normal emission.

The present result points out important considerations when measuring photoelectron spectra of fullerenes and other molecular materials. The symmetry effects in the AD must be considered when determining the mean-free path in bulk systems.[36,37] Adsorbing C_{60} on a metal surface, and monitoring the substrate valence-band intensity, implicitly assumes that the AD is unaltered after adsorption of the molecular overlayer, which is trivially true only for core levels.

For metallic fullerene samples such as K_3C_{60}, the effects elucidated here could become enhanced, since inelastic scattering with a low first plasmon frequency[41] does not necessarily remove the photoelectron from the spectrum. Thus it becomes increasingly important to make use of the molecular distribution when acquiring such data. In particular, measuring close to normal emission, and especially, close to the direction of polarization, will minimize the effects of inelastic scattering on the spectral shapes at low binding energies. We show elsewhere that this is indeed the case for K_3C_{60}.[42] This aspect holds also for monolayers, since the intralayer inelastic scattering (in the simple model developed here) damps the high-angle portions of the angular distribution. We anticipate that studies of other molecular materials will benefit from such considerations.

ACKNOWLEDGMENTS

We thank R. Fasel for stimulating and helpful discussions. This work was supported by the CARAMEL consortium, which received funding from Stiftelsen för Strategisk Forskning. We would also like to acknowledge Vetenskapsrådet and Göran Gustafsons Stiftelse for financial support.

*Electronic address: joachim.schiessling@fysik.uu.se

†Present address: Max-Lab, University of Lund, Box 118, SE-221 00 Lund, Sweden.

‡Electronic address: Paul.Bruehwiler@empa.ch

[1] S. Hüfner, *Photoelectron Spectroscopy* (Springer-Verlag, Berlin, 1996).

[2] G.A. Sawatzky, Nature (London) **342**, 480 (1989).

[3] S.V. Borisenko, M.S. Golden, S. Legner, T. Pichler, C. Dürr, M. Knupfer, J. Fink, G. Yang, S. Abell, and H. Berger, Phys. Rev. Lett. **84**, 4453 (2000).

[4] J.H. Weaver, J.L. Martins, T. Komeda, Y. Chen, T.R. Ohno, G.H. Kroll, N. Troullier, R.E. Haufler, and R.E. Smalley, Phys. Rev. Lett. **66**, 1741 (1991).

[5] R.W. Lof, M.A. van Veenendaal, B. Koopmans, H.T. Jonkman, and G.A. Sawatzky, Phys. Rev. Lett. **68**, 3924 (1992).

[6] P. Rudolf, M.S. Golden, and P.A. Brühwiler, J. Electron Spectrosc. Relat. Phenom. **100**, 409 (1999).

[7] O. Gunnarsson, Rev. Mod. Phys. **69**, 575 (1997).

[8] V. Brouet, H. Alloul, T.-N. Le, S. Garaj, and L. Forró, Phys. Rev. Lett. **86**, 4680 (2001).

[9] J. Wu, Z.-X. Chen, D.S. Dessau, R. Cao, D.S. Marshall, P. Pianetta, I. Lindau, X. Yang, J. Terry, D.M. King, B.O. Wells, D. Elloway, H.R. Wendt, C.A. Brown, H. Hunziker, and M. de Vries, Physica C **157**, 251 (1992).

[10] G. Gensterblum, J.-J. Pireaux, P.A. Thirty, R. Caudano, T. Buslaps, R.L. Johnson, G.L. Lay, V. Aristov, R. Günter, A. Taleb-Ibrahimi, G. Indlekofer, and Y. Petroff, J. Electron Spectrosc. Relat. Phenom. **81**, 89 (1996).

[11] P.J. Benning, C.G. Olson, D.W. Lynch, and J.H. Weaver, Phys. Rev. B **50**, 11 239 (1994).

[12] M. Merkel, M. Knupfer, M.S. Golden, J. Fink, R. Seemann, and R.L. Johnson, Phys. Rev. B **47**, 11 470 (1993).

[13] G. Gensterblum, J. Electron Spectrosc. Relat. Phenom. **81**, 89 (1996).

[14] E.L. Shirley and S.G. Louie, Phys. Rev. Lett. **71**, 133 (1993).

[15] S.G. Louie and E.L. Shirley, J. Phys. Chem. Solids **54**, 1767 (1993).

[16] P.J. Benning, D.M. Poirier, N. Troullier, J.L. Martins, J.H. Weaver, R.E. Haufler, L.P.F. Chibante, and R.E. Smalley, Phys. Rev. B **44**, 1962 (1993).

[17] T. Liebsch, O. Plotzke, F. Heiser, U. Hergenhahn, O. Hemmers, R. Wehlitz, J. Viefhaus, B. Langer, S.B. Whitfield, and U. Becker, Phys. Rev. A **52**, 457 (1995).

[18] M. Venuti, M. Stener, G.D. Alti, and P. Decleva, J. Chem. Phys. **111**, 4589 (1999).

[19] P. Decleva, S. Furlan, G. Frozoni, and M. Stener, Chem. Phys. Lett. **348**, 363 (2001).

[20] Y.B. Xu, M.Q. Tan, and U. Becker, Phys. Rev. Lett. **76**, 3538 (1996).

[21] T. Liebsch, O. Plotzke, R. Hentges, A. Hempelmann, U. Hergenhahn, F. Heiser, J. Viefhaus, U. Becker, and Y. Xu, J. Electron Spectrosc. Relat. Phenom. **79**, 419 (1996).

[22] S. Hasegawa, T. Miyamae, K. Yakushi, H. Inokuchi, K. Seki, and N. Ueno, Phys. Rev. B **58**, 4927 (1998).

[23] B.N. Jensen, S.M. Butorin, T. Kaurila, R. Nyholm, and L.I. Johansson, Nucl. Instrum. Methods Phys. Res. A **394**, 243 (1997).

[24] A.J. Maxwell, P.A. Brühwiler, D. Arvantis, J. Hasselström, and N. Mårtensson, Chem. Phys. Lett. **260**, 71 (1996).

[25] H. Bethe, *Handbuch der Physik* (Springer-Verlag, Berlin, 1933).

[26] J.W. Cooper and S.T. Manson, Phys. Rev. **177**, 157 (1969).

[27] P. Decleva (private communication).

[28] C.S. Fadley, R.J. Baird, W. Siekhaus, T. Novakov, and S.Å.L. Bergström, J. Electron Spectrosc. Relat. Phenom. **4**, 93 (1974).

[29] A. Jablonski and C.J. Powell, J. Electron Spectrosc. Relat. Phenom. **100**, 137 (1999).

[30] D. Naumović, A. Stuck, T. Greber, J. Osterwalder, and L. Schlapbach, Phys. Rev. B **47**, 7462 (1993).

[31] M. S. Dresselhaus, G. Dresselhaus, and P. C. Eklund, *Science of Fullerenes and Carbon Nanotubes* (Academic Press, San Diego, CA, 1996).

[32] A.J. Maxwell, P.A. Brühwiler, A. Nilsson, N. Mårtensson, and P. Rudolf, Phys. Rev. B **49**, 10 717 (1994).

[33] This is consistent with the localization of core holes observed in aromatic systems, discussed recently in, e.g., Ref. 34, and is the basis for x-ray photoelectron diffraction measurements on ordered fullerene monolayers (Ref. 35).

[34] P.A. Brühwiler, O. Karis, and N. Mårtensson, Rev. Mod. Phys. **74**, 703 (2002).

[35] R. Fasel, P. Aebi, R.G. Agostino, D. Naumovic, J. Osterwalder, A. Santaniello, and L. Schlapbach, Phys. Rev. Lett. **76**, 4733 (1996).

[36] A. Goldoni, L. Sangaletti, F. Parmigiani, G. Comelli, and G. Paolucci, Phys. Rev. Lett. **87**, 076401 (2001).

[37] G.K. Wertheim, D.N.E. Buchanan, E.E. Chaban, and J.E. Rowe, Solid State Commun. **83**, 785 (1992).

[38] Note that the inelastic-scattering effects in the model developed here are equivalent to those obtained in the continuum model if $R \rightarrow 0$ or $\lambda \rightarrow \infty$.

[39] V.I. Nefedov, J. Electron Spectrosc. Relat. Phenom. **100**, 1 (1999).

[40] J.L. Martins, N. Troullier, and J.H. Weaver, Chem. Phys. Lett. **180**, 475 (1991).

[41] M. Knupfer, M. Merkel, M.S. Golden, J. Fink, O. Gunnarsson, and V.P. Antropov, Phys. Rev. B **47**, 13 944 (1993); A.I. Lichtenstein, O. Gunnarsson, M. Knupfer, J. Fink, and J.F. Armbruster, J. Phys.: Condens. Matter **8**, 4001 (1996).

[42] J. Schiessling, L. Kjeldgaard, T. Käämbre, I. Marenne, L. Qian, J. N. O'Shea, J. Schnadt, M. G. Garnier, D. Nordlund, M. Nagasono, C. Glover, P. Rudolf, J.-E. Rubensson, N. Mårtensson, J. Nordgren, and P. A. Brühwiler (unpublished).